

ANALYZING THE DIMENSIONS OF PREATTENTIVE VISUAL SENSITIVITY

Charles Chubb, Ian Scofield, George Sperling
Department of Cognitive Sciences, UC Irvine

Corresponding author:

Charles Chubb
Department of Cognitive Sciences
UC Irvine
Irvine, CA 92697-5100
cfchubb@uci.edu
949-824-1481

Abstract

Perhaps the most fundamental question in vision science is: Which physical differences in the visual input are spontaneously visible and which are not? At present this question remains unanswered. The answer will take the form of a Table of Dimensions of Preattentive Visual Sensitivity, or DPVS Table. The DPVS table may ultimately prove as important to theories of visual processing as the periodic table of elements has been to theories of chemistry. This paper describes psychophysical methods for deriving the DPVS Table. In particular, for a given domain of physical variation—e.g., achromatic light intensity, these methods enable one to (1) determine the number of preattentive visual mechanisms that are differentially sensitive to variations in the domain and (2) derive the principal components of the space of physical variations to which those mechanisms are sensitive.

1 Introduction

The methods developed in this paper are predicated on several assumptions about low level vision. First, we assume that the initial segmentation of the visual field antecedent to deriving object boundaries, identities, locations, etc. uses a battery of fast, spatially parallel image transformations whose response images reflect “the amounts of various kinds of visual substances present in the image” (Adelson & Bergen, 1991). It is convenient to imagine these substance-sensing transformations as being implemented in retinotopically organized neural arrays; in any one of these arrays all neurons apply the same computation to the visual input but at different locations in the retina. Thus each array works continuously like a movie camera to capture a “neural image” (Robson, 1980) mapping the changing distribution of a particular “visual substance.” We call these neural image transformations “preattentive mechanisms,” or just “mechanisms,” because we assume that they operate automatically outside conscious control. The high cost in neural resources of a single mechanism makes it likely that human vision has only a modest number, suggesting that we may be able to figure out how many there are and what they sense.

We assume that a target region is preattentively discriminated from a background only if the two regions differentially activate one or more mechanisms. For example, if they differentially activate one or more cone classes, target and background will be discriminable due to a difference in brightness or color.

In addition, however, since the work of Julesz (1962, 1975, 1981) and Beck (1966, 1982), it has been recognized that human vision has mechanisms sensitive to purely textural properties (see also Beck, Sutter & Ivry, 1987; Graham, 1989; Gurnsey & Browse, 1989; Julesz & Bergen, 1983). For example, in Fig. 1, the texture elements (or texels) of the test patch on the left differ in orientation from those of the background but not in spatial frequency, whereas the texels of the patch on the right differ in spatial frequency but not in orientation; in each case the test patch pops out from the background. Whenever two textures spontaneously segregate, this means they differentially activate one or more mechanisms. Many models of preattentive texture segregation have been offered (e.g., Beck, Prazdny, & Rosenfeld, 1983; Bergen & Landy, 1991; Bovik, Clark & Geisler, 1990; Caelli, 1985; Fogel & Sagi, 1989; Graham, 1989, 1991; Graham, Beck & Sutter, 1992; Grossberg & Mingolla, 1985; Knutsson & Granlund, 1983; Landy & Bergen, 1991; Malik & Perona, 1990; Wilson, 1993). All propose that human vision embodies a number of mechanisms sensitive to local pattern orientation and spatial frequency. Often the proposed mechanisms use spatially local linear filtering followed by rectification. Julesz (1962) famously conjectured that all preattentive texture discrimination used linear filtering followed by a squaring nonlinearity. And indeed, spectral energy accounts well for many cases of preattentive texture discrimination (Bergen & Adelson, 1988); however, many counterexamples exist (Diaconis & Freedman, 1981; Julesz,

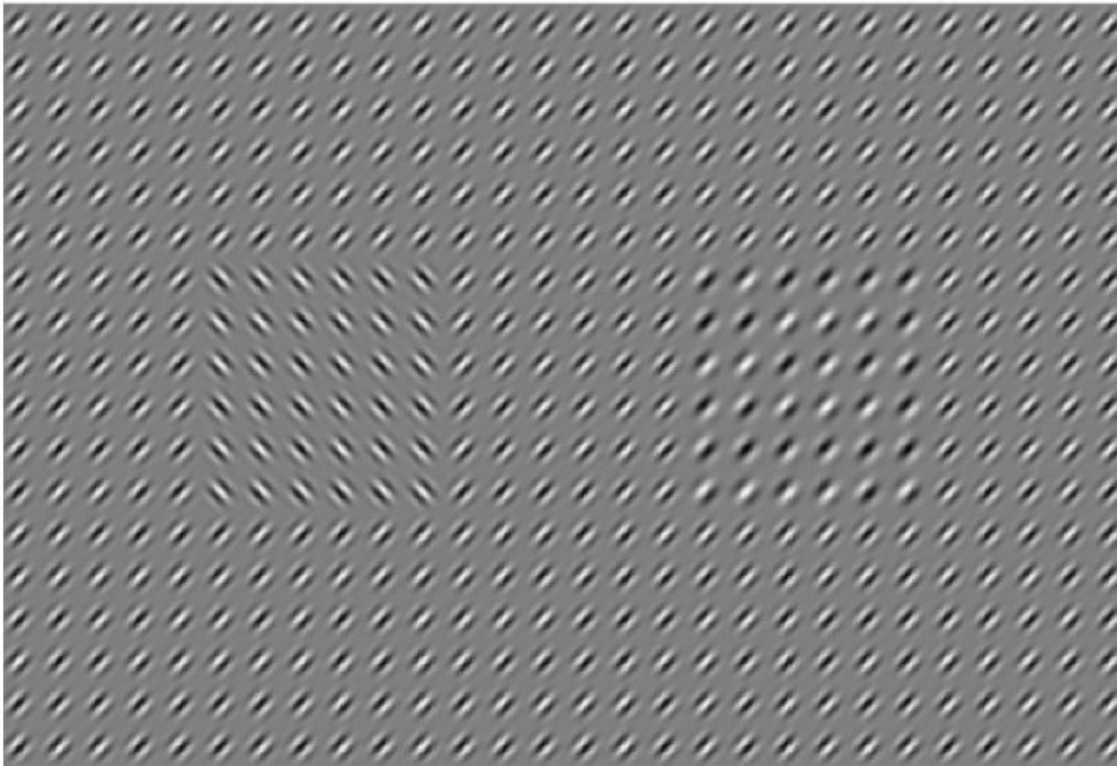


Figure 1: Preattentive texture segregation driven by orientation (left) and spatial frequency (right)

Gilbert, Shepp, & Frisch, 1973; Julesz, Gilbert, & Victor, 1978, Pollack, 1971a,b, 1972, 1973). Although such examples and the models proposed to explain them are suggestive, little progress has been made in actually measuring the dimensions of preattentive visual sensitivity. The main obstacle has been lack of a method. The point of this paper is to fill this void.

2 Groundwork

The methods we describe use psychophysical tasks that require the observer to discriminate one sort of texture from another. Any of various different discrimination tasks would work: for example, the observer might be asked to (1) identify the location of a target patch of one kind of texture in a background of another, or (2) identify the orientation of a square wave grating whose bars alternated between two different kinds of texture, or (3) indicate which of several distinct patches of texture was different from the others. For our purposes the particular discrimination task is not important.

What are important are the types of textures we use and how we manipulate the differences between them. These are described next.

2.1 Scrambles

We always start with a particular set Ω of micropatterns. A micropattern is a “mini-image” that can serve as a single component in a large patch of texture. We write N_Ω for the number of micropatterns in Ω . Fig. 2 shows several possible micropattern sets. It will be useful to distinguish

three general classes of micropattern sets: linear, cyclic and unordered sets. The empirical questions of interest and the methods of analysis are likely to differ between these three different types of micropattern set. Figs. 2a and b are examples of linear micropattern sets. Fig. 2c is an example of a cyclic micropattern set, and 2d is an example of an unordered set. Linear and cyclic micropattern sets both conform to an obvious ordering, whereas unordered sets do not. On the other hand, linear sets have a unique pair of opposite, extreme elements whereas cyclic sets do not.

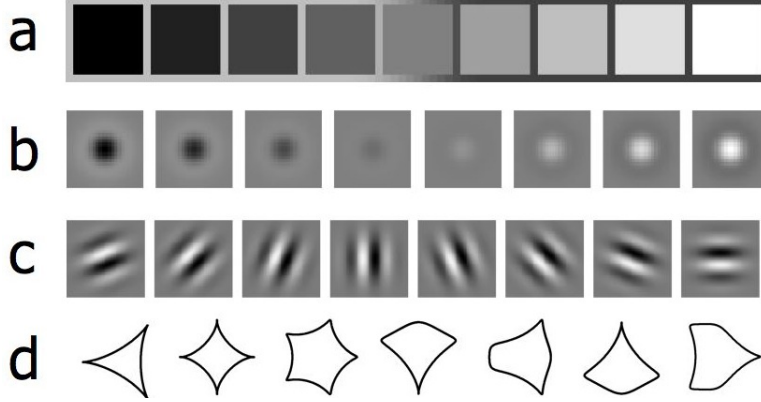


Figure 2: Four different sets of micropatterns. (a) the linear set $\Omega_{Contrast}$, (b) another linear set, (c) a cyclic set, (d) an unordered set.

To generate a scramble from a micropattern set Ω we first specify the proportions $p(\omega)$ with which different micropatterns $\omega \in \Omega$ appear in the scramble. Then we load a “virtual urn” with exactly the number of micropatterns needed to tile the stimulus region in exactly (or as nearly as possible) the proportions $p(\omega)$; then we draw from the urn randomly without replacement to assign micropatterns to the texel locations of the scramble. We call probability distribution p the scramble histogram. Fig. 3 shows some examples of scrambles using micropattern set of Fig. 2a. The inset bar plots show the histograms.

We write $U(\omega)$ for the uniform histogram on Ω —i.e., the histogram that assigns the value $\frac{1}{N_\Omega}$ to all $\omega \in \Omega$. The scramble shown in Fig. 3a has histogram U . By default we treat real-valued functions of Ω as a column vectors, writing $g^T h$ for the inner product of functions $g, h : \Omega \rightarrow \mathbb{R}$. That is

$$g^T h = \sum_{\omega \in \Omega} g(\omega)h(\omega). \quad (1)$$

Note that for any function $g : \Omega \rightarrow \mathbb{R}$, $g^T U$ is the mean value of g .

We call any real-valued function $\phi : \Omega \rightarrow \mathbb{R}$ a (histogram) perturbation if it sums to 0. Note that:

1. The difference between any two histograms is a perturbation.
2. any perturbation ϕ is orthogonal to U —i.e. ϕ 's mean value, $\phi^T U$, is 0.
3. $U + \phi$ is a histogram if and only if ϕ is a perturbation whose minimum value is greater than or equal to $-\frac{1}{N_\Omega}$; thus, $U + \phi$ and $U - \phi$ are both histograms if and only if the maximum absolute value of ϕ is less than or equal to $\frac{1}{N_\Omega}$. For this reason, we call any perturbation ϕ *maximal* if its maximum absolute value is $\frac{1}{N_\Omega}$.

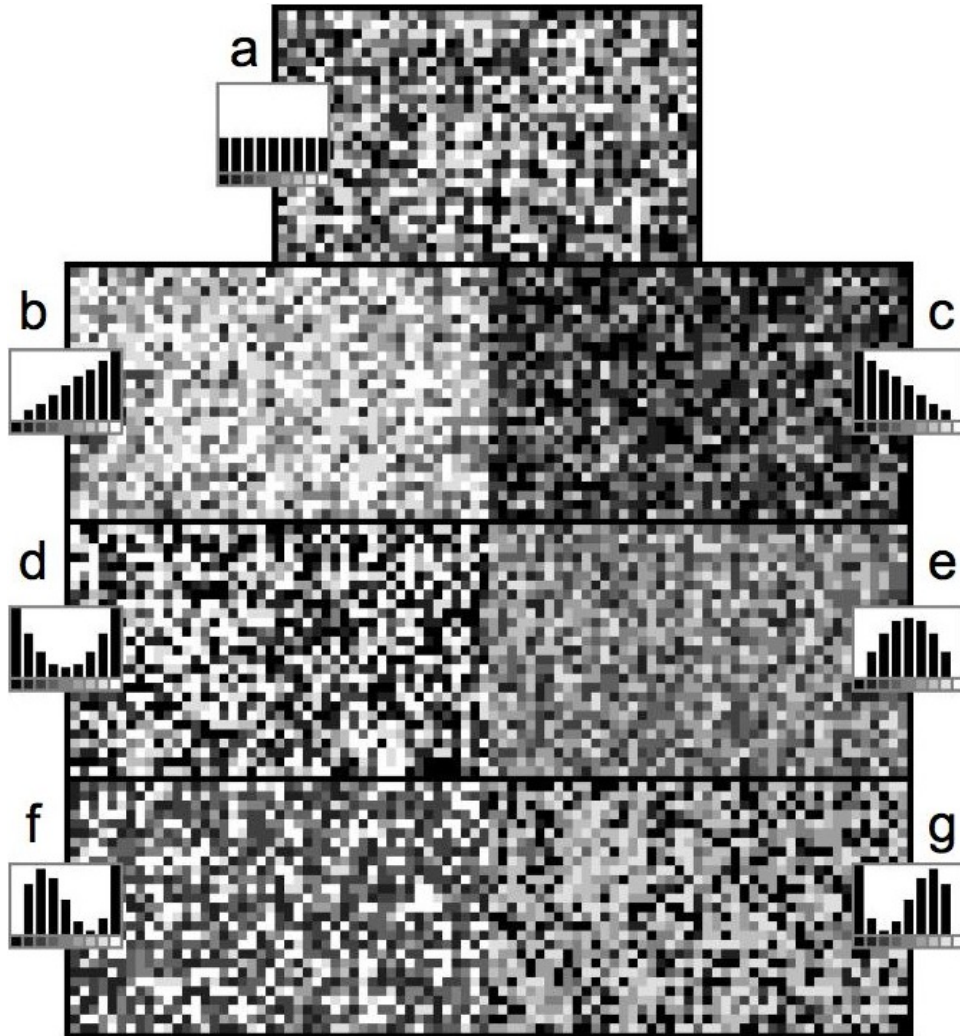


Figure 3: Scrambles of $\Omega_{Contrast}$, with (a) histogram U , (b) and (c) U plus complementary linear perturbations, (d) and (e) U plus complementary quadratic perturbations, (f) and (g) complementary cubic perturbations. The linear, quadratic and cubic perturbations used here are mutually orthogonal.

2.2 An example task

The methods we describe will work with many different discrimination tasks. We describe a simple one here to aid intuition. In this 4 alternative, forced choice task, on every trial the observer is asked to try to detect the orientation of a square wave grating whose bars are filled with two different types of Ω -scramble. Specifically, for a number of reasons (discussed in Chubb, Econopouly & Landy, 1994), it is useful to use scrambles that are perturbed away from the uniform histogram U in opposite directions. In other words, on every trial, we choose some perturbation ϕ and set the histograms of the target and background scrambles equal to $U + \phi$ and $U - \phi$. Four example stimuli are shown in Fig. 4, one in each of the four possible orientations. The square waves in each of the two upper stimuli alternate between the two types of scramble shown in Fig. 3b and c; The lower left stimulus alternates between the two scrambles shown in Fig. 3d and e, and the lower right stimulus alternates between the two scrambles shown in Fig. 3f and g.

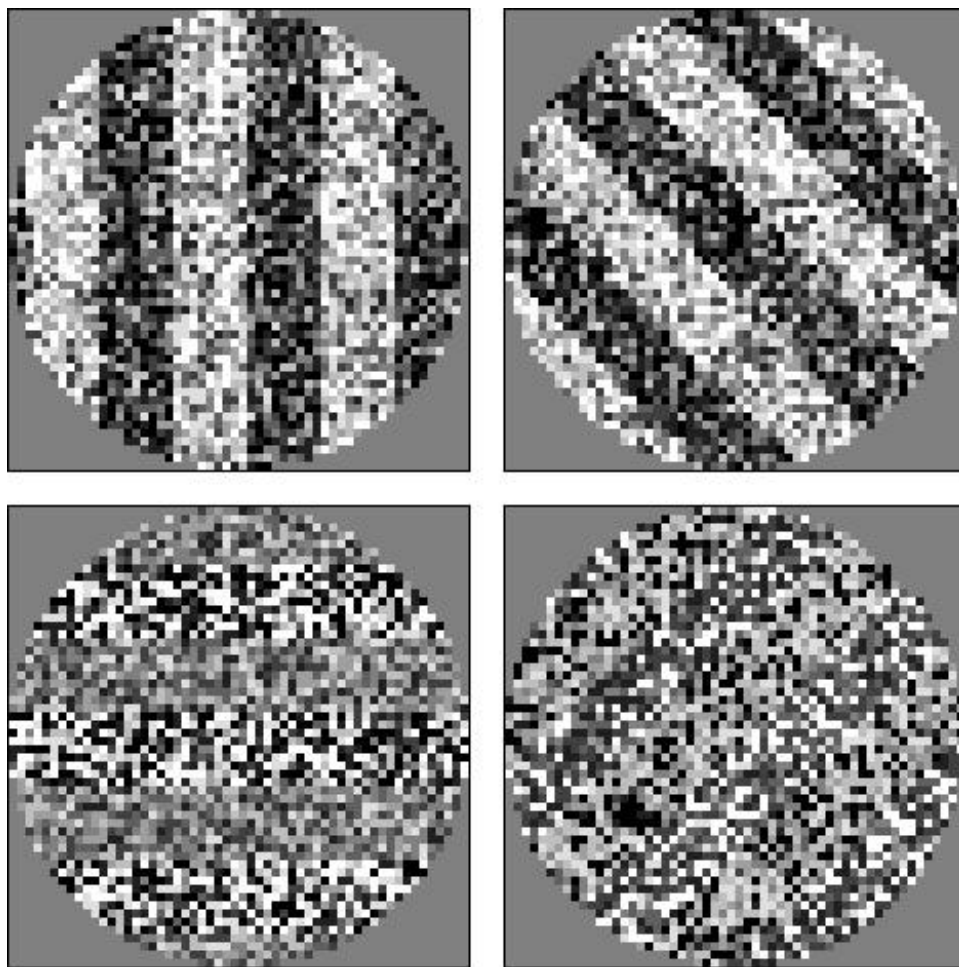


Figure 4: Four example stimuli using the scrambles shown in Fig. 3. The task is a 4AF orientation judgment. The two upper stimuli alternate between scrambles of the types shown in Fig. 3b and c. The lower left stimulus alternates between the two scrambles shown in Fig. 3d and e, and the lower right stimulus alternates between the two scrambles shown in Fig. 3f and g.

As discussed below (Sec. 4), by choosing perturbations ϕ appropriately, one can derive a basis spanning the space of all physical variations to which people are differentially sensitive in a given

domain. We call this the differential sensitivity space of the domain.

3 Differential sensitivity functions and spaces.

3.1 Thinking about a single mechanism.

We picture any mechanism M as being realized in the brain by a retinotopically organized array of neurons; that is, the neurons in M are arranged in the brain in an array, and the location in the array of a neuron reflects the location in the retina of the neuron’s receptive field. Each neuron in the M -array uses the same (possibly complicated, nonlinear) computation to derive its response from the pattern of light in its receptive field. This computation defines the “visual substance” M senses.

We assume implicitly that the visual substance sensed by M is at least moderately “fine-grained”; that is, the neurons in the M -array must have relatively small receptive fields, and whatever lateral interactions occur between them must be restricted in the scope of their influence. If so, then any neuron in M will be driven mainly by input in a small region of the retina, and the resulting neural image will carry relatively high acuity information. Otherwise, the neural image captured by M is likely to be too blurry to be useful.

When an Ω scramble stimulates the M -array, any given micropattern in the scramble is certain to influence the responses of multiple M neurons. On the one hand, neurons close to each other in M are likely to have overlapping receptive fields. Thus, wherever a micropattern $\omega \in \Omega$ occurs, it cannot avoid impinging upon the receptive fields of multiple M neurons. In addition, each micropattern is spatially extended; thus its impact spreads to include neurons whose receptive fields do not overlap. Finally, M ’s neurons may laterally interact. If so, then a given micropattern can indirectly influence the activation levels of M -neurons by stimulating the receptive fields of M -neurons with lateral connections to them.

When an Ω scramble stimulates the M -array, different micropatterns of the same type are likely to produce different effects in M . The most important reason for this is that M ’s response to a given $\omega \in \Omega$ is likely to be somewhat context-dependent, and the contexts of two identical micropatterns within the scramble will almost always differ. To take an extreme (and aberrant) case, suppose M neurons were very highly activated by a pair of abutting micropatterns if the left one were of type ω and the right one were of type ω' but not at all by any other combinations. In this case, the influence exerted on M neurons by a micropattern of type ω would depend crucially on whether the micropattern to the right of it in the scramble was of type ω' . Although this scenario is possible, we would not expect such a mechanism to play a very important role in enabling discrimination of Ω scrambles because the right sorts of abutting micropattern pairs would occur very rarely in any scramble. Rather, we expect that scramble discrimination will be most powerfully enabled by those mechanisms affording differential sensitivity to different $\omega \in \Omega$ that is largely immune to variations in micropattern context. For our purposes, all that matters about any such mechanism M are the average effects produced in M by different types of micropatterns $\omega \in \Omega$. We next turn to the task of formalizing “first-order” sensitivity of this sort. However, first we introduce the following basic concept from linear algebra.

3.2 The projection of a function into a subspace.

Let S_1, S_2, \dots, S_N be orthogonal subspaces of the space of all real-valued functions of a micropattern set Ω . (I.e., any function in one of these subspaces is orthogonal to all functions in all of the other subspaces.) If the sum of the dimensions of the S_k ’s is equal to N_Ω , then any function $g : \Omega \rightarrow \mathbb{R}$

can be expressed as a unique sum

$$g = \sum_{k=1}^N g_k \quad (2)$$

where $g_k \in S_k$ for $k = 1, 2, \dots, N$. For each k , the function g_k is called the *projection of g into S_k* .

It is straightforward to derive the projection of g into any given subspace S . One first obtains an orthonormal basis b_1, b_2, \dots, b_n of S (e.g., using the Gram-Schmidt method). Then for B the matrix whose columns are the b_k 's, the projection of g into S is given by

$$Proj_S(g) = BB^T g = \sum_{k=1}^n (b_k^T g) b_k. \quad (3)$$

Note that each of the terms $(b_k^T g) b_k$ is the projection of g into the one-dimensional subspace spanned by b_k .

3.3 The differential sensitivity function of a mechanism.

Returning to the mechanism M : for any $\omega \in \Omega$, let $f_{total}(\omega)$ be the mean activation produced in M by an occurrence of ω in a scramble. Thus, the mean M activation produced by a scramble with histogram p is:

$$\sum_{\omega \in \Omega} f_{total}(\omega) p(\omega) = f_{total}^T p. \quad (4)$$

Then define the *differential sensitivity function* of M to be the projection f of f_{total} into the space of all perturbations. Since the difference between any histograms p and q is a perturbation, we see that the difference in mean M activation produced by scrambles with histograms p and q is

$$f_{total}^T p - f_{total}^T q = f_{total}^T (p - q) = f^T (p - q). \quad (5)$$

Thus, in particular for any perturbation ϕ , the difference in mean M activation produced by scrambles with histograms $U + \phi$ vs. $U - \phi$ is $2f^T \phi$.

3.4 The differential sensitivity space of a micropattern set Ω

In general we expect human vision to have multiple mechanisms that are differentially sensitive to the different ω 's in a given micropattern set Ω . Let $f_1, f_2, \dots, f_{N_{Mechs}}$ be the differential sensitivity functions of these mechanisms. Then we call the f_k 's the differential sensitivity functions of Ω and the space they span the Ω differential sensitivity space.

3.5 Assumptions about how mechanisms combine to control discrimination.

Suppose F is the matrix whose column vectors are the Ω differential sensitivity functions. Then for any perturbation ϕ , the k^{th} entry of the vector $2F^T \phi$ gives the difference in mean activation produced in the k^{th} mechanism by scrambles with histograms $U + \phi$ vs $U - \phi$. We make the standard assumption that discrimination performance is a psychometric function of the Minkowski norm of $2F^T \phi$ for some exponent β : i.e., of

$$Sal(\phi) = 2 \left(\sum_k |f_k^T \phi|^\beta \right)^{\frac{1}{\beta}}, \quad (6)$$

where $Sal(\phi)$ is short for “salience” of ϕ .

If $\beta = 2$, then the salience of a given perturbation ϕ is the $2|F^T\phi|$ (i.e., twice the Euclidean length of $F^T\phi$), and equiperformance contours are parallel ellipses centered at 0. This case is particularly important because discrimination data tend to conform to such ellipses in practice. This has been observed for temporal contrast modulations (Rashbass, 1970; Watson & Nachmias, 1977), spatial contrast modulations (Logvinenko, 1993; Manahilov & Simpson, 2001), chromatic modulations (Knoblauch & Maloney, 1996; Noorlander & Koenderink, 1983; Poirson, Wandell, Varner & Brainard, 1990; Poirson & Wandell, 1990,1996), and texture modulations (Victor, Chubb & Conte, 2004). The discussion in Sec. 4 assumes that $\beta = 2$; however, as we show in the appendix, the method we describe is robust with respect to broad violations of this assumption.

We assume that salience is linked to discrimination performance by a psychometric function that we model as a Weibull function. For any perturbation ϕ , we assume probability correct at “discriminating ϕ ” (our shorthand locution for “discriminating scrambles with histograms $U + \phi$ and $U - \phi$ ”) is given by

$$\Psi(Sal(\phi)) = 0.25 + 0.75 \left[1 - e^{-Sal(\phi)^\gamma} \right]. \quad (7)$$

The reader will note that this Weibull function has only one free parameter, the exponent γ that controls the function’s steepness. Typically, the Weibull function also includes a second parameter A that enters as a divisor to the argument, $Sal(\phi)$. This parameter is redundant in our model because it can be absorbed by the matrix F hidden in the definition of $Sal(\phi)$.

4 Deriving the principal components of the Ω differential sensitivity space

We now describe how to derive the principal components of the Ω differential sensitivity space for an arbitrary micropattern set Ω . This method is new, remarkably powerful, and very general in scope of application. The description in this section is terse, our main purpose being to provide an overview of the logic; in Sec. 5 we show how to use the method with a step-by-step example.

4.1 Seed-expansion: a method for finding an element of the differential sensitivity space

If human vision has significant sensitivity to Ω , then there will exist at least one perturbation that affords superthreshold discrimination. We normalize such a perturbation to obtain the function b_1 and then measure the amplitude α_1 such that $\rho = \alpha_1 b_1$ yields threshold discrimination. In addition, let $b_2, b_3, \dots, b_{N_\Omega-1}$ be orthonormal perturbations, all also orthonormal with respect to b_1 .

To make the logic of our method clear, we assume in this section that $Sal(\phi) = 2|F^T\phi|$ for any perturbation ϕ . Under this assumption, as we now show, we can derive one function that resides in the Ω differential sensitivity space. However the appendix shows that the definition of salience can be greatly generalized, and the seed expansion method will still produce an element the Ω differential sensitivity space.

We will measure the form of the following real-valued function of Ω :

$$f_\rho = FF^T\rho. \quad (8)$$

Note that f_ρ is a linear combination of the columns of F and hence is an element of the differential sensitivity space. We call ρ the *seed* perturbation of f_ρ , and f_ρ the *expansion* of ρ .

To derive f_ρ we will first measure all of the inner products, $f_\rho^T b_k$, $k = 1, \dots, N_\Omega - 1$. Then we use Eq. 3 to derive f_ρ .

For purposes of measuring the unknown inner products, note first that for any perturbation ϕ and any nonnegative scalar A ,

$$Sal(A\phi) = ASal(\phi). \quad (9)$$

This holds regardless of the exponent β in Eq. 6. In addition (here we use the stronger assumption that $Sal(\phi) = |F^T \phi|$), note that

$$\begin{aligned} Sal(\rho + \phi)^2 - Sal(\rho - \phi)^2 &= 4(\rho + \phi)^T F F^T (\rho + \phi) - 4(\rho - \phi)^T F F^T (\rho - \phi) \\ &= 16\rho^T F F^T \phi \\ &= 16f_\rho^T \phi \end{aligned} \quad (10)$$

It is convenient to take the 0.724 threshold because this makes threshold salience equal to $\Psi^{-1}(0.724) = 1$. Thus, since $\rho = \alpha_1 b_1$ yields threshold performance, we obtain

$$f_\rho^T b_1 = \rho^T F F^T b_1 = \rho^T F F^T \frac{\rho}{\alpha_1} = \frac{Sal(\rho)^2}{4\alpha_1} = \frac{1}{4\alpha_1}. \quad (11)$$

Next, to estimate $f_\rho^T b_k$ for a given $k > 1$, we choose a small scalar ϵ and construct the perturbations

$$\eta_k^+ = \rho + \epsilon b_k \quad \text{and} \quad \eta_k^- = \rho - \epsilon b_k. \quad (12)$$

We then measure the rescaling factors α_k^+ and α_k^- required to make each of $\alpha_k^+ \eta_k^+$ and $\alpha_k^- \eta_k^-$ yield threshold discrimination.¹ Thus,

$$Sal(\alpha_k^+ \eta_k^+) = Sal(\alpha_k^- \eta_k^-) = 1, \quad (13)$$

from which Eq. 9 implies that

$$Sal(\rho + \epsilon b_k) = \frac{1}{\alpha_k^+} \quad \text{and} \quad Sal(\rho - \epsilon b_k) = \frac{1}{\alpha_k^-}. \quad (14)$$

Combining Eqs. 10 and 14 we obtain the result we will use to estimate our inner products:

$$f_\rho^T b_k = \frac{Sal(\rho + \epsilon b_k)^2 - Sal(\rho - \epsilon b_k)^2}{16\epsilon} = \frac{1}{16\epsilon} \left[\left(\frac{1}{\alpha_k^+} \right)^2 - \left(\frac{1}{\alpha_k^-} \right)^2 \right]. \quad (15)$$

We can then use the estimates of $f_\rho^T b_k$ provided by Eqs. 15 and 11 to derive the expansion,

$$f_\rho = \sum_{k=1}^{N_\Omega-1} (f_\rho^T b_k) b_k. \quad (16)$$

4.2 A note on the robustness of the seed-expansion method.

In the Appendix we adopt a much more general model of the salience computation (the model given in Eq. 22) and show that even in this case, as $\epsilon \rightarrow 0$ in Eq. 15, the function f_ρ implicitly defined by the inner products $f_\rho^T b_k$ is an element of the Ω differential sensitivity space. Thus, if the value of ϵ we use in Eq. 15 is small, this method is likely to be robust to failures of the assumption that salience is given by Eq. 6 with $\beta = 2$.

¹We refer to α_k^+ and α_k^- as “rescaling factors” to avoid any confusion. In particular, it would be misleading to refer to α_k^+ and α_k^- as perturbation “amplitudes” which might suggest either that they were the norms or the maximum absolute values of $\alpha_k^+ \eta_k^+$ and $\alpha_k^- \eta_k^-$. They are neither of these. They are the factors by which η_k^+ and η_k^- must be rescaled to achieve threshold performance.

4.3 Using seed-expansion to measure the principal components of the differential sensitivity space.

As above, let F be the $N_\Omega \times N_{mechs}$ matrix whose column vectors are the differential sensitivity functions of Ω . Applying singular value decomposition to F yields $SV D^T = F$ for (unique) column orthonormal $N_\Omega \times N_{mechs}$ matrices S and D and (unique) $N_{mechs} \times N_{mechs}$ diagonal matrix V . Thus $FF^T = SV D D^T V^T S^T = SV^2 S^T$. Note the implication that f_ρ does not depend on D . Ultimately, this means that we can determine F only up to an arbitrary assignment of D . What we CAN determine using our methods are S and V . The diagonal entries of V^2 are the eigenvalues of FF^T , and the column vectors of S are the corresponding eigenvectors, also known as the *principal components* of the differential sensitivity space.

We will derive FF^T and then apply singular value decomposition to FF^T to obtain the principal components S and associated eigenvalues V^2 . To derive FF^T we will need to iterate the seed-expansion N_{mechs} times. We proceed as follows.

We first check whether there exist any maximal perturbations that yield superthreshold discrimination. If not, then human vision has no mechanisms with significant sensitivity to Ω . If so, we select such a perturbation and adjust its amplitude to obtain a perturbation ρ_1 that yields threshold discrimination. We use ρ_1 as our first seed and derive the expansion f_{ρ_1} . We then test whether there exist any perturbations orthogonal to f_{ρ_1} that support superthreshold discrimination. If so, then once again we choose one of them and adjust its amplitude to obtain another perturbation ρ_2 that yields threshold discrimination. We use this as a second seed and derive the expansion f_{ρ_2} .

We reiterate this process as many times as needed: after step k we test whether the space of perturbations orthogonal to all the previously derived expansions, $f_{\rho_1}, f_{\rho_2}, \dots, f_{\rho_k}$, contains a perturbation that yields superthreshold discrimination. If so, we choose such a perturbation, adjust its amplitude to obtain a new seed ρ_{k+1} that yields threshold discrimination and derive the expansion $f_{\rho_{k+1}}$. If not, then we conclude that $N_{mechs} = k$ and that the expansions $f_{\rho_1}, f_{\rho_2}, \dots, f_{\rho_{N_{mechs}}}$ form a basis of the differential sensitivity space.

We can use this basis to derive FF^T . We first construct a matrix R whose first N_{mechs} columns are the seed perturbations $\rho_k, k = 1, 2, \dots, N_{mechs}$ and whose last $N_\Omega - N_{mechs}$ columns span the space of all vectors orthogonal to the expansions $f_{\rho_1}, f_{\rho_2}, \dots, f_{\rho_{N_{mechs}}}$. Note first that R is a square ($N_\Omega \times N_\Omega$) matrix of full rank and thus has an inverse. Next construct the matrix Q whose first N_{mechs} columns are the expansions $f_{\rho_1}, f_{\rho_2}, \dots, f_{\rho_{N_{mechs}}}$ and whose last $N_\Omega - N_{mechs}$ columns are all zero. Note also that $FF^T R$ is equal to the matrix Q . We thus derive

$$FF^T = QR^{-1}. \quad (17)$$

Finally, we apply singular value decomposition to FF^T to derive the principal components of the Ω differential sensitivity space and their associated eigenvalues.

5 An example application

The purpose of this section is to illustrate how we actually measure a differential sensitivity space. As we proceed, we will address several important practical issues not discussed in the abstract description of the method above. In this section, we focus on textures composed of small squares of different Weber contrasts, as illustrated in Figs. 3 and 4.

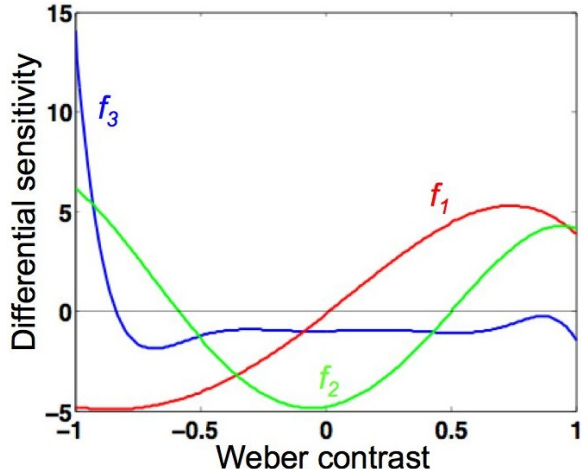


Figure 5: The differential sensitivity functions of three hypothetical mechanisms enabling discrimination of Weber contrast scrambles. These mechanisms are consistent with previous findings (Chubb, Econopouly & Landy, 1994; Chubb, Landy & Econopouly, 2004; Chubb et al., 2006).

5.1 The example mechanisms.

In this example, we assume three mechanisms consistent with previous research (Chubb, Econopouly & Landy, 1994; Chubb, Landy & Econopouly, 2004; Chubb et al., 2006). The sensitivity functions of these three mechanisms are shown in Fig. 5. These three functions form a basis of the human differential sensitivity space for scrambles of small squares varying in gray level. We also assume that $Sal(\phi) = |F^T \phi|$ where F is the matrix whose column vectors are the three differential sensitivity functions, f_1 , f_2 and f_3 . Finally, we assume probability correct in our 4AFC orientation discrimination task is given by Eq. 7 with $\gamma = 2.0$, approximately in line with the results of Chubb, Econopouly & Landy, 2004.

5.2 Selecting the micropattern set.

In this example, the domain v of physical variation being investigated is continuous. The first question one must answer with this sort of physical domain is: How finely should the micropattern set Ω sample the domain? (or equivalently, how large should we take N_Ω ?) This decision should be made carefully for several reasons:

1. One needs to be confident that N_Ω is greater than the number N_{Mechs} of mechanisms differentially sensitive to Ω scrambles. Otherwise, it will be impossible either to derive a basis spanning the Ω differential sensitivity space or to determine its dimension.
2. Another reason to make N_Ω moderately large is the following: if one or more mechanisms has sensitivity that varies rapidly as a function of v , then if N_Ω is too small, one may fail to detect those variations.
3. On the other hand, if N_Ω is small, then scrambles can have higher concentrations of the different kinds of micropatterns in Ω , and one can experimentally vary these concentrations over a larger range. As this suggests, the smaller one makes Ω , the easier it tends to be to generate scrambles that are strongly discriminable, and the easier it is to measure sensitivities to those scrambles.

We have found that taking N_Ω around 9 often works well. However, the particular choice will depend on factors specific to the domain of physical variation under study. In our simulations, we take $\Omega = \{-1.0, -0.75, -0.5, -0.25, 0, 0.25, 0.5, 0.75, 1.0\}$. Thus, $N_\Omega = 9$.

5.3 Using seed-expansion to derive the principal components of the Ω differential sensitivity space

To empirically estimate the the principal components of the Ω differential sensitivity space we will need to expand three different seeds, ρ_1, ρ_2, ρ_3 . The three resulting expansions, $f_{\rho_1}, f_{\rho_2}, f_{\rho_3}$, should span (within measurement error) the Ω differential sensitivity space. Thus, we should find that the space of perturbations orthogonal to all of f_{ρ_1}, f_{ρ_2} and f_{ρ_3} affords very weak discrimination (if any).

For our first seed we can use any perturbation we wish provided it can be scaled to yield threshold discrimination. In the current simulation we use the third order, discrete domain Legendre polynomial λ_3 shown in Fig. 6 (aong with the other Legendres). These polynomials, $\lambda_1, \lambda_2, \dots, \lambda_{N_\Omega-1}$ are often useful in scramble experiments. They are derived by applying Gram-Schmidt orthonormalization to the vectors $v_k(\omega) = \omega^k$, for $k = 0, 1, \dots, N_\Omega - 1$. (We throw out $\lambda_0(\omega)$, which is the constant function $= \frac{1}{\sqrt{N_\Omega}}$ and therefore not a perturbation.) For any k between 1 and $N_\Omega - 1$, the perturbations $\lambda_1, \lambda_2, \dots, \lambda_k$ span the space of all polynomial perturbations of order less than or equal to k .

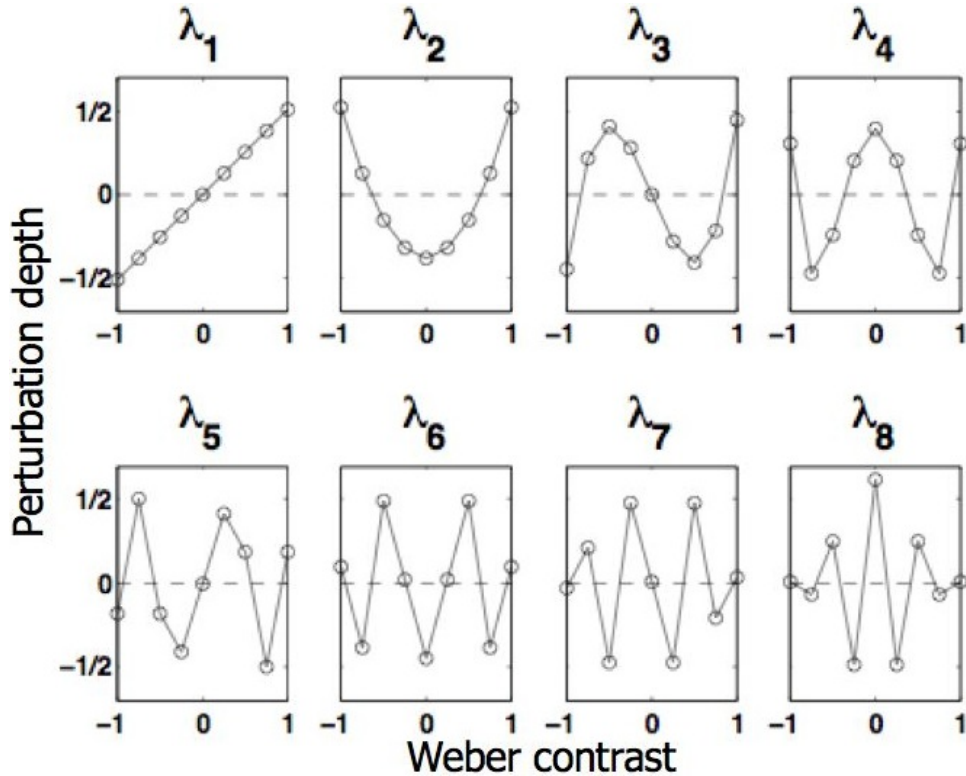


Figure 6: Discrete domain Legendre polynomials of order 1 to 8. They form an orthogonal basis of the space of all perturbations.

We first use a 300-trial, 2-up/1-down staircase to estimate the threshold amplitude α_1 for discriminating $b_1 = \lambda_3$ and use this estimate to scale λ_3 to derive our first seed perturbation,

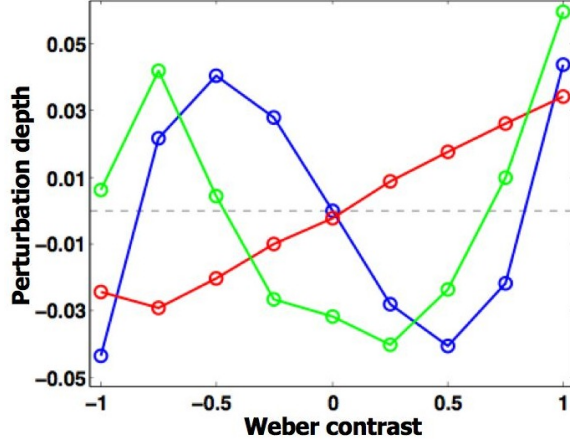


Figure 7: The three seeds used in deriving the principal components of the Ω differential sensitivity space. The first, second and third seeds are given by the blue, red and green curves.

shown by the blue curve in Fig. 7. In the current simulation, this estimate turns out to be $\alpha_1 = 0.098$.

5.3.1 Expanding the first seed

To apply the seed expansion method (Sec. 4.1) in the current situation, let $b_1 = \lambda_3$, $b_2 = \lambda_1$, $b_3 = \lambda_2$, $b_4 = \lambda_4$, $b_5 = \lambda_5$, $b_6 = \lambda_7$, $b_7 = \lambda_7$ and $b_8 = \lambda_8$ (where it is understood that $|\lambda_k| = 1$ for $k = 1, 2, \dots, 8$).

To derive the expansion f_ρ we need to estimate the dot products $f_\rho^T b_k$ for $k = 1, 2, \dots, 8$. In accordance with Eq. 11, we note that

$$f_\rho^T b_1 = \frac{1}{4\alpha_1} = 1.57. \quad (18)$$

To derive $f_\rho^T b_k$ for $k > 1$, we need first to construct the perturbations η_k^+ and η_k^- (Eq. 12). This requires us to choose a value of ϵ . (In the current simulations we use $\epsilon = 0.3|\rho| = 0.0294$.) Next we need to measure the rescaling factors α_k^+ and α_k^- for which $\alpha_k^+ \eta_k^+$ and $\alpha_k^- \eta_k^-$ yield threshold discrimination. We can then apply Eq. 15 to estimate $f_\rho^T b_k$ for $k = 2, 3, \dots, 8$.

Fig. 8 shows how we estimate the thresholds α_k^+ and α_k^- . Each of the seven subfigures represents a planar subspace of perturbations. Points (x, y) correspond to perturbations $\phi_{(x,y)} = x\lambda_k + y\lambda_3$, with k equal to 1, 2, 4, 5, 6, 7, 8 in the different subplots. Note that because $|\lambda_k| = 1$ for all k , the Euclidean distance of any point (x, y) from the origin is equal to the norm of the corresponding perturbation. In each subplot, the blue line shows the boundary of realizable perturbations. (That is, each perturbation on this boundary has maximum absolute value equal to $1/9$.) The middle of the three black markers on the $\lambda_3 (= b_1)$ axis marks the location $(0, \alpha_1)$, which corresponds to the seed perturbation ρ ; the bracketing markers give the associated 95% Bayesian credible interval for α_1 .² These markers are reproduced in all subplots. Note that the markers in each subplot are symmetric around the origin; this is because the task is to discriminate scrambles with histograms

²In this simulation, all threshold estimates are medians of estimated Bayesian posterior distributions, and bracketing markers give the 2.5 and 97.5 percentiles of these same distributions. In each case, uniform priors are used on all model parameters, with a range that far exceeds plausible values, and the Metropolis-Hastings algorithm is used to derive a sample of size 12000 from the posterior density. The first 2000 samples are discarded.

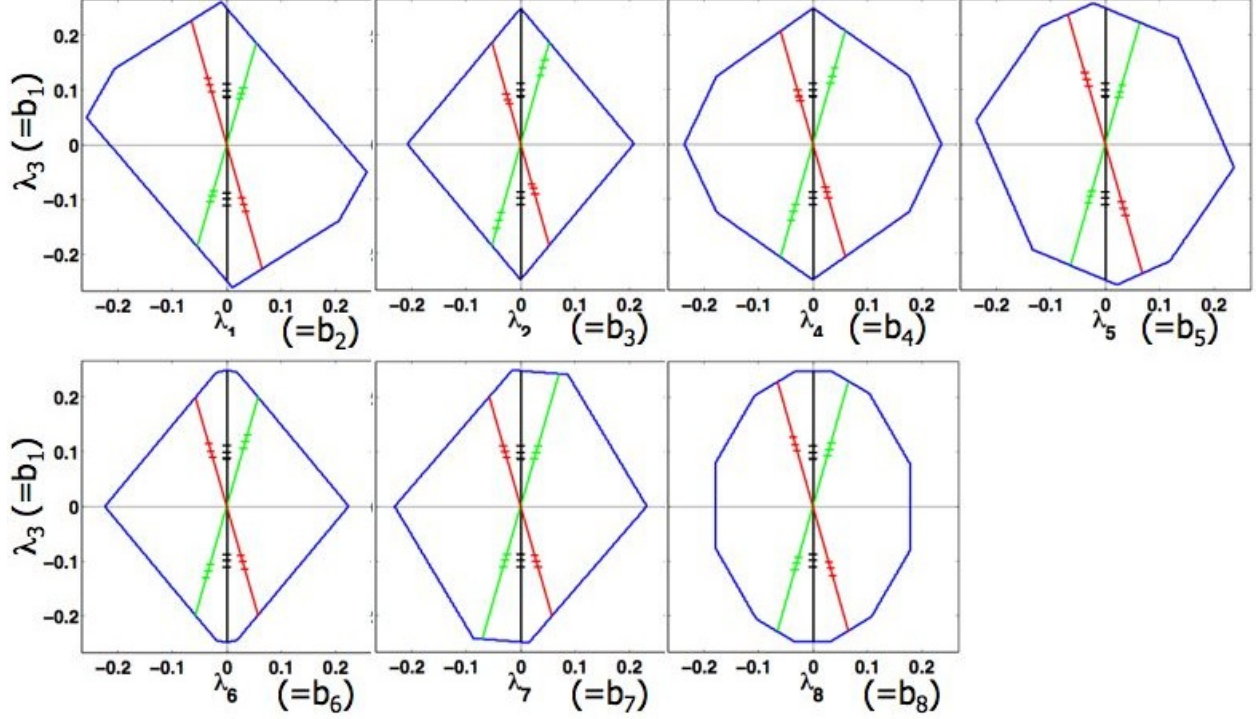


Figure 8: Estimates of threshold perturbations $\alpha_k^+ \eta_k^+$ (along green lines) and $\alpha_k^- \eta_k^-$, (along red lines). Threshold estimates are medians of Bayesian posterior distributions. Upper and lower markers give 95% credible intervals. Thresholds are duplicated above and below the horizontal axis because points symmetric with respect the origin correspond to the same judgement. Each threshold is estimated from 300 trials of a 2-up/1-down staircase. The black markers on the λ_3 axis (identical in all plots) give the estimate of threshold α_1 (and associated 95% credible intervals) for discriminating $\alpha_1 \lambda_3 = \rho_1$.

$U + \phi_{(x,y)}$ and $U - \phi_{(x,y)} = U + \phi_{(-x,-y)}$. Thus points on opposite sides of the origin correspond to the same discrimination task.

The green line in a given subplot is the locus of realizable scalar multiples of η_k^+ , and the red line is the locus of realizable scalar multiples of η_k^- . We conduct a simulated 2-up/1-down staircase to collect psychometric data along each of these loci. In each subplot, the interval along the green (or red) line from the origin to the upper blue line is split into 100 steps (this number was not chosen with any care); the staircase starts at step 50 and is run for 300 trials. The three markers on the green line in the subplot for basis element b_k , $k = 2, 3, \dots, 8$ give the estimated value of $\gamma_k^+ = \alpha_k^+ \eta_k^+$ bracketed by its 95% credible interval; similarly, the three markers on the red line give the estimate of $\gamma_k^- = \alpha_k^- \eta_k^-$ bracketed by its credible interval. Thus, to derive estimates of α_k^+ and α_k^- we need to take

$$\alpha_k^+ = \frac{|\gamma_k^+|}{|\eta_k^+|} \quad \text{and} \quad \alpha_k^- = \frac{|\gamma_k^-|}{|\eta_k^-|} \quad (19)$$

Using these threshold estimates, we obtain our first basis element

$$Q_1 = \sum_{k=1}^7 (f_\rho^T b_k) b_k \quad (20)$$

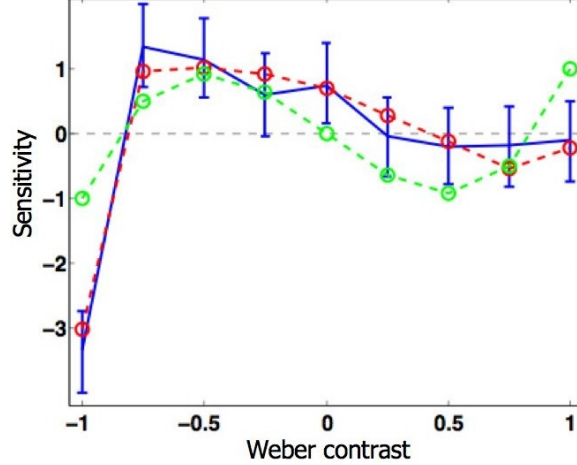


Figure 9: The first basis element, Q_1 . This is the expansion of the seed perturbation $\rho = 0.098\lambda_3$. Error bars are 95% Bayesian credible intervals. The dashed green line shows the contribution to the expansion of the seed perturbation.

where

$$f_\rho^T b_1 = \frac{1}{4\alpha_1} \quad \text{and} \quad f_\rho^T b_k = \frac{1}{16\epsilon} \left[\left(\frac{1}{\alpha_k^+} \right)^2 - \left(\frac{1}{\alpha_k^-} \right)^2 \right], \quad k = 2, 3, 4, 5, 6, 7. \quad (21)$$

Q_1 is plotted by the blue line in Fig. 9. Error bars are 95% Bayesian credible intervals. The dashed red line gives the actual value of the expansion f_ρ estimated by Q_1 . The dashed green line shows the contribution to the expansion of the seed perturbation.

5.3.2 Expanding the second seed

We use as our second seed the perturbation ρ that results from orthogonalizing λ_1 with respect to the first expansion Q_1 (shown by the red curve in Fig. 7). Again the amplitude of ρ is fixed by using a 300-trial 2-up/1-down staircase to estimate the threshold perturbation norm for discriminating ρ . In the current simulation, this threshold estimate is $\alpha_1 = 0.0646$. Then we set $b_1 = \frac{\rho}{|\rho|}$, $b_2 = \frac{Q_1}{|Q_1|}$, and select the rest of b_3, \dots, b_8 so that all of b_1, b_2, \dots, b_8 are orthonormal perturbations.

To derive the expansion Q_2 of ρ we use exactly the same method as we did to derive Q_1 ; the only difference was that in this case we used $\epsilon = 0.0452$, which yields smaller credible intervals around the resulting expansion, Q_2 , shown in Fig. 10. In this figure error bars are 95% Bayesian credible intervals; the dashed red line gives the actual value of the expansion estimated by Q_2 ; and the dashed green line shows the contribution to Q_2 of the seed perturbation.

5.3.3 Deriving the third basis function

We use almost exactly the same method to derive Q_3 as we did to derive Q_2 . The only difference is that we choose our third seed (shown by the green curve in Fig. 7) to be orthogonal to the first two seeds (the red and blue curves in this figure). We set $b_1 = \frac{Q_3}{|Q_3|}$, $b_2 = \frac{Q_1}{|Q_1|}$, $b_3 = \frac{Q_2}{|Q_2|}$, and then fill out b_4, \dots, b_8 with 5 additional mutually orthonormal perturbations. For this expansion, we set $\epsilon = 0.029$.

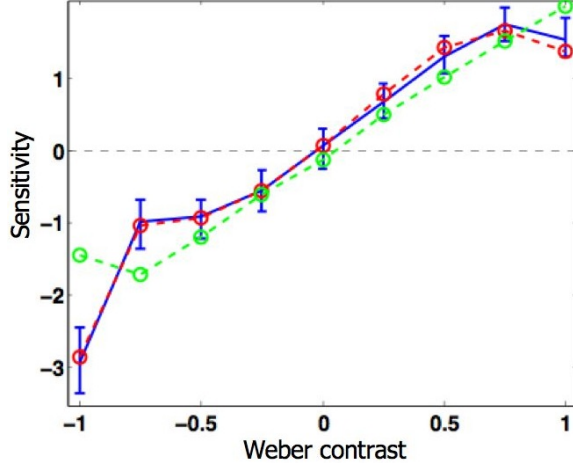


Figure 10: The second expansion Q_2 . The dashed red line shows the true expansion of the second seed. The solid blue line shows the estimated expansion with 95% Bayesian credible intervals. The dashed green line shows the contribution of the seed itself to the expansion.

5.3.4 Testing the residual space of perturbations

After each iteration of the seed-expansion method, one must check that there still exists some perturbation orthogonal to the previously obtained basis functions that affords superthreshold discrimination. We have not emphasized this stage in previous iterations because the maximum amplitude forms of each of the perturbations used as seeds for the second and third basis functions yield obvious discrimination. For ϕ equal to either of Q_2 or Q_3 scaled to its maximum physically realizable level, a glance at a square wave modulating between scrambles with histograms $U + \phi$ and $U - \phi$ would immediately reveal that discrimination will be superthreshold in our standard task.

However, after extracting the expansions Q_1 , Q_2 and Q_3 , the standard procedure fails to disclose any perturbations orthogonal to Q_1 , Q_2 and Q_3 that yield obvious superthreshold discrimination. As above, let $v(\omega)$ be the Weber contrast of micropattern ω . We apply Gram-Schmidt orthonormalization to the sequence of functions $g_1 = U$, $g_2 = Q_1$, $g_3 = Q_2$, $g_4 = Q_3$, $g_5 = v$, $g_6 = v^2$, $g_7 = v^3$, $g_8 = v^4$, and $g_9 = v^5$. The last five of the functions, $b_{4,1}$, $b_{4,2}, \dots, b_{4,5}$, that result from this operation are orthonormal perturbations, and all are orthogonal to Q_1 , Q_2 and Q_3 . If Q_1 , Q_2 and Q_3 exactly spanned the differential sensitivity space of Ω , then each of $b_{4,k}$, $k = 1, 2, \dots, 5$ would yield chance discrimination. However, due to measurement error, this is not true. In the current simulation, these perturbations scaled to their maximum physically realizable levels are predicted to yield discrimination success probabilities, 0.30, 0.28, 0.28, 0.26, and 0.35. Thus, even though discrimination performance is not at chance in all cases, the residual space gives us no obvious seed perturbation to expand into an additional basis function. We take this as our signal to stop.

5.4 Deriving the principal components

Finally we apply the method of Sec 4.3 to estimate the principal components of the Ω differential sensitivity space. We first construct the matrices Q and R as prescribed. That is: Q has as its first three column vectors the expansions, Q_1 , Q_2 and Q_3 , and six additional columns all filled with zeros. R has as its first three columns the three seed perturbations shown by the blue, red and green curves in Fig. 7 and its remaining six columns filled by vectors R_4, \dots, R_9 , that are mutually

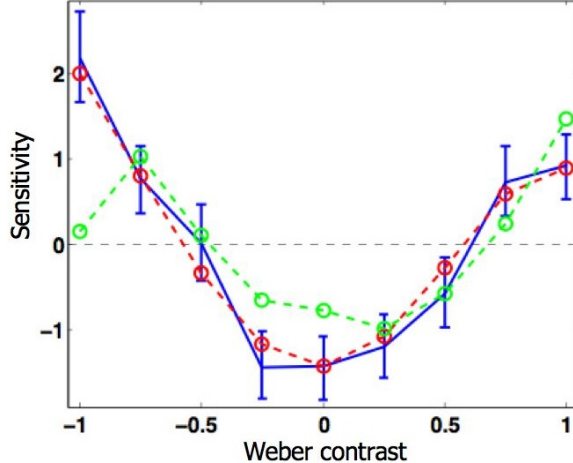


Figure 11: The third expansion, Q_3 . The estimate of Q_3 is shown by the blue line (along with 95% Bayesian credible intervals). The dashed red line shows the true expansion of the third seed (shown by the green line in Fig. 7). The dashed green line shows the contribution of the seed itself to the expansion.

orthonormal and orthogonal to all of the three seeds. Then we apply Eq. 17 to derive an estimate $\widehat{FF^T}$ of the covariance matrix FF^T . Finally, we apply singular value decomposition to derive the matrices S and V for which $SV^2S^T = \widehat{FF^T}$. The estimated principal components we seek are the three nonzero column vectors of SV . These are plotted in Fig. 12.

6 Summary

Perhaps the most basic question in visual perception is: which physical variations in the pattern of light presented to the retina are spontaneously visible? At present, this question is still without an answer. In this paper, we have described and demonstrated a method that can be used to answer this question for the space of textures that can be made by taking random arrangements micropatterns drawn in different proportions from a given set Ω . Such textures are called scrambles. If human vision has mechanisms M_1, M_2, \dots, M_N that are differentially sensitive to scrambles, then the methods we have described can be used to derive the principal components of the space spanned by the functions f_1, f_2, \dots, f_N that give the sensitivities of these mechanisms to the different micropatterns in Ω . The method described relies on a new technique called “seed expansion” (see Sec. 4.1) that can be used to extract an element of the differential sensitivity space.

We used the method in a simulated experiment, showing how to derive the principal components of the differential sensitivity space of a micropattern set Ω by iterative seed-expansion.

By applying the methods we have described across a range of different micropattern sets Ω it should be possible to derive a table of Dimensions of Preattentive Visual Sensitivity. Such a table will be fundamental to the future development of vision science.

7 Acknowledgements

Special thanks to Charless Fowlkes for useful comments on an earlier version of this paper.

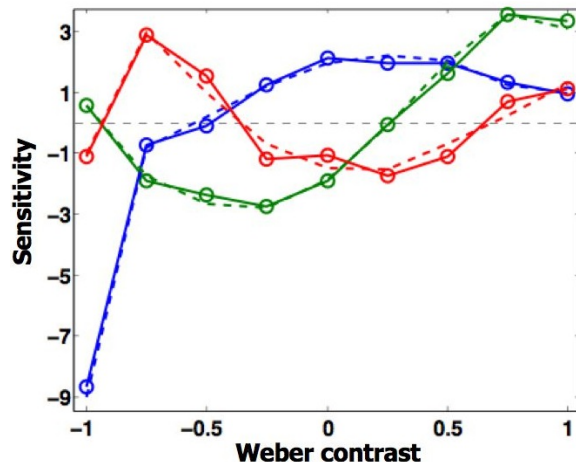


Figure 12: The estimated principal components of the Ω differential sensitivity space (shown by solid lines with circles). The dashed lines give the actual principal components.

REFERENCES

- Adelson, E. H., & Bergen, J. R. (1991). The plenoptic function and the elements of early vision. In M. S. Landy, & J. A. Movshon (Eds.), *Computational models of visual processing*. (pp. 3–20). Cambridge, MA: MIT Press.
- Beck, J. (1966). Perceptual grouping produced by changes in orientation and shape. *Science*, *154*, 538—540.
- Beck, J. (1982). Textural Segmentation. In J. Beck (Ed.), *Organization and Representation in Perception* (pp. 285–317). Hillsdale, NJ: Erlbaum.
- Beck, J., Prazdny, K., & Rosenfeld, A. (1983). A theory of textural segmentation. In J. Beck, B. Hope, & A. Rosenfeld (Eds.), *Human and Machine Vision* (pp. 1–38). New York, Academic Press.
- Beck, J., Sutter, A., & Ivry, R. (1987). Spatial frequency channels and perceptual grouping in texture segregation. *Computer Vision, Graphics, and Image Processing*, *37*, 299–325.
- Bergen, J. R., & Adelson, E. H. (1988). Visual texture segmentation based on energy measures. *Journal of the Optical Society of America A*, *3*, 98–101.
- Bergen, J. R., & Landy, M. S. (1991). The computational modeling of visual texture segregation. In M. S. Landy, & J. A. Movshon (Eds.), *Computational Models of Visual Processing* (pp. 253–271). Cambridge, MA: MIT Press.
- Bovik, A. C., Clark, M., & Geisler, W. S. (1990). Multichannel texture analysis using localized spatial filters. *IEEE Transactions on Pattern Analysis and Machine Intelligence*, *12*, 55–73.
- Caelli, T. (1985). Three processing characteristics of visual texture segmentation. *Spatial Vision*, *1*, 19–30.
- Chubb, C., Econopouly, J., & Landy, M. S. (1994). Histogram contrast analysis and the visual segregation of IID textures. *Journal of the Optical Society of America A*, *11*, 2350–2374.

- Chubb, C., & Landy, M. S. (1991). Orthogonal distribution analysis: A new approach to the study of texture perception. In M. S. Landy, & J. A. Movshon (Eds.), *Computational models of visual processing* (pp. 291–301). Cambridge, MA: MIT Press.
- Chubb, C., M. S. Landy, J. Econopouly (2004). A visual mechanism tuned to black, *Vision Research*, *44*, 3223–3232, 2004.
- Chubb, C, Nam, J-H, Bindman, D.R., Sperling, G. (2007) The Three Dimensions of Human Visual Sensitivity to First-order Contrast Statistics, *Vision Research*, *47*, 2237–2248.
- Diaconis, P. & Freedman, D. (1981). On the Statistics of Vision: The Julesz conjecture. *J. Math Psych.*, *24*, 112–118.
- Fogel, I., & Sagi, D. (1989). Gabor filters as texture discriminators. *Biological Cybernetics*, *61*, 103–113.
- Knoblauch, K., & Maloney, L. T. (1996). Testing the indeterminacy of linear color mechanisms from color discrimination data. *Vision Research*, *36*, 295–306.
- Graham, N. (1989). *Visual Pattern Analyzers*. New York: Oxford.
- Graham, N. (1991). Complex channels, early local nonlinearities, and normalization in texture segregation. In M. S. Landy, & J. A. Movshon (Eds.), *Computational Models of Visual Processing* (pp. 273–290). Cambridge, MA: MIT Press.
- Graham, N., Beck, J., & Sutter, A. (1992). Nonlinear processes in spatial-frequency channel models of perceived texture segregation: Effects of sign and amount of contrast. *Vision Research*, *32*, 719–743.
- Grossberg, S., & Mingolla, E. (1985). Neural dynamics of perceptual grouping: textures, boundaries, and emergent segmentations. *Perception & Psychophysics*, *38*, 141–171.
- Gurnsey, R., & Browse, R. A. (1989). Asymmetries in visual texture discrimination. *Spatial Vision*, *4*, 31–44.
- Julesz, B. (1962). Visual pattern discrimination. *IRE Transactions on Information Theory*, *IT-8*, 84–92.
- Julesz, B. (1975). Experiments in the visual perception of texture. *Scientific American*, April, 34–43.
- Julesz, B. (1981). Textons, the elements of texture perception, and their interactions. *Nature*, *290*, 91–97.
- Julesz, B., & Bergen, J. R. (1983). Textons, the fundamental elements in preattentive vision and perception of textures. *Bell System Technical Journal*, *62*, 1619–1645.
- Julesz, B., Gilbert, E. N., Shepp, L. A., & Frisch, H. L. (1973). Inability of humans to discriminate between visual textures that agree in second order statistics. *Perception*, *2*, 391–405.
- Julesz, B., Gilbert, E. N., & Victor, J. D. (1978). Visual discrimination of textures with identical third order statistics. *Biological Cybernetics*, *31*, 137–149.

- Knutsson, H., & Granlund, G. H. (1983). Texture analysis using two-dimensional quadrature filters. In *Proceedings of the IEEE Computer Society Workshop on Computer Architecture for Pattern Analysis and Image Database Management* (pp. 206–213). Silver Spring, MD: IEEE Computer Society.
- Landy, M. S., & Bergen, J. R. (1991). Texture segregation and orientation gradient. *Vision Research*, *31*, 679–691.
- Logvinenko, A. D. (1993). Failure of convexity of some threshold curves for compound grating: Implications for the modern models of visual pattern detection. *Biological Cybernetics*, *70*, 55–64.
- Malik, J., & Perona, P. (1990). Preattentive texture discrimination with early vision mechanisms. *Journal of the Optical Society of America A*, *7*, 923–932.
- Manahilov, V., & Simpson, W. A. (2001). Energy model for contrast detection: Spatial-frequency and orientation selectivity in grating summation. *Vision Research*, *41*, 1547–1560.
- Noorlander, C., & Koenderink, J. J. (1983). Spatial and temporal discrimination ellipsoids in colour space. *Journal of the Optical Society of America A*, *14*, 1533–1543.
- Poirson, A. B., & Wandell, B. A. (1990). The ellipsoidal representation of spectral sensitivity. *Vision Research*, *30*, 647–652.
- Poirson, A. B., & Wandell, B. A. (1996). Pattern-color separable pathways predict sensitivity to simple colored patterns. *Vision Research*, *36*, 512–526.
- Poirson, A. B., Wandell, B. A., Varner, D., & Brainard, D.H. (1990). Surface characterizations of color thresholds The ellipsoidal representation of spectral sensitivity. *J. Opt. Soc. Am. A*, *7*, 783–789.
- Pollack, I. (1971a). Detection of one-, two-, and three-dimensional Markov constraints in visual displays. *Acta Psychologica*, *35*, 219–232.
- Pollack, I. (1971b). Perception of two-dimensional Markov constraints within visual displays. *Perception and Psychophysics*, *9*, 461–464.
- Pollack, I. (1972). Visual discrimination thresholds for one- and two- dimensional Markov spatial constraints. *Perception and Psychophysics*, *12*, 161–167.
- Pollack, I. (1973). Discrimination of third-order Markov constraints within visual displays. *Perception and Psychophysics*, *13*, 276–280.
- Rashbass, C. (1970). The visibility of transient changes of luminance. *Journal of Physiology*, *210*, 165–186.
- Robson, J. G. (1980). Neural images: The physiological basis of spatial vision. In C. S. Harris (Ed.), *Visual Coding and Adaptability* (pp. 177–214). Hillsdale, NJ: Erlbaum.
- Victor, J. D., C. Chubb, M. M. Conte (2005). Interaction of luminance and higher order statistics in texture discrimination, *Vision Research*, *45*, 311–328.
- Wilson, H. R. (1993). Nonlinear processes in visual pattern discrimination. *Proceedings of the National Academy of Sciences, USA*, *90*, 9785–9790.

Watson, A. B., & Nachmias, J. (1977). Patterns of temporal interaction in the detection of gratings. *Vision Research*, 17, 893–902.

APPENDIX: Concerning the robustness of the method for deriving a basis of the differential sensitivity space

In this section, we show that the method described in section 4 for deriving a basis of the differential sensitivity space for a given micropattern set Ω will work no matter how mechanism responses are combined to determine the salience of a texture difference. We begin by adopting a very general model of salience. As in 4, let F be the matrix whose column vectors are the (unknown) differential sensitivity functions f_k of the mechanisms enabling discrimination of Ω -scrambles. Then for any perturbation ϕ we shall assume only that

$$Sal(\phi) = H \left(\sum_{k=1}^N G_k (f_k^T \phi) \right) \quad (22)$$

for differentiable functions H and G_1, G_2, \dots, G_N (where N is the number of mechanisms differentially sensitive to Ω -scrambles). This definition includes the Minkowski length (Eq. 6) as a special case. In particular, if $G_k(x) = |x|^\beta$ for all k , and $H(x) = x^{\frac{1}{\beta}}$, then $Sal(\phi)$ is the Minkowski length of $F^T \phi$ with exponent β .

Our method for deriving a basis hinges on our ability to extract a single perturbation f_ρ that is an element of the Ω differential sensitivity space.

What we need to show is that there exists an element f_ρ of the Ω differential sensitivity space such that for any perturbation ϕ ,

$$\frac{\widehat{Sal}(\rho + \epsilon\phi)^2 - \widehat{Sal}(\rho - \epsilon\phi)^2}{4\epsilon} \approx f_\rho^T \phi \quad (23)$$

provided ϵ is made small enough. If we can establish this, we take an orthonormal basis $b_1, b_2, \dots, b_{N_\Omega-1}$ of perturbations and use Eq. 23 to derive each of the inner products $f_\rho^T b_k$, $k = 1, 2, \dots, b_{N_\Omega-1}$; then we can synthesize $f_\rho = \sum_k (f_\rho^T b_k) b_k$. We assume that enough trials have been run that $\widehat{Sal}(\phi) \approx Sal(\phi)$. Therefore, we can secure Eq. 23 by proving the following

Theorem.

If $Sal(\phi)$ is given by Eq. 22, then for any modulators ρ and ϕ

$$\lim_{\epsilon \rightarrow 0} \left(\frac{Sal(\rho + \epsilon\phi)^2 - Sal(\rho - \epsilon\phi)^2}{4\epsilon} \right) = f_\rho^T \phi \quad (24)$$

for

$$f_\rho = c_\rho F g_\rho, \quad (25)$$

where (using the prime notation for the derivative) c_ρ is the scalar given by

$$c_\rho = Sal(\rho) H' \left(\sum_k G_k (f_k^T \rho) \right) \quad (26)$$

and g_ρ is the column vector whose k^{th} component is

$$g_{\rho,k} = G'_k (f_k^T \rho). \quad (27)$$

Before we present the proof, note that f_ρ given by Eq. 25 is a linear combination of the columns of F and is therefore an element of the Ω differential sensitivity space and hence eligible to serve as an element in a basis of this space.

Proof. It will be convenient to set

$$q(x) = Sal(\rho + x\phi)^2 \quad (28)$$

and

$$r(x) = q(x) - q(-x). \quad (29)$$

Four applications of the chain rule to the right side of Eq. 28 yield

$$q'(x) = 2Sal(\rho + x\phi)H' \left(\sum_k G_k (f_k^T [\rho + x\phi]) \right) \sum_k G'_k (f_k^T [\rho + x\phi]) f_k^T \phi. \quad (30)$$

Because $r'(x) = 2q'(x)$ it follows that

$$r'(0) = 2q'(0) = 4Sal(\rho)H' \left(\sum_k G_k (f_k^T \rho) \right) \sum_k G'_k (f_k^T \rho) f_k^T \phi = 4f_\rho^T \phi \quad (31)$$

for f_ρ given by Eq. 25. On the other hand, the definition of the derivative yields

$$r'(x) = \lim_{\epsilon \rightarrow 0} \left(\frac{(Sal(\rho + [x + \epsilon]\phi))^2 - Sal(\rho - [x + \epsilon]\phi)^2) - (Sal(\rho + x\phi)^2 - Sal(\rho - x\phi)^2)}{\epsilon} \right) \quad (32)$$

implying that

$$r'(0) = \lim_{\epsilon \rightarrow 0} \left(\frac{Sal(\rho + \epsilon\phi)^2 - Sal(\rho - \epsilon\phi)^2}{\epsilon} \right). \quad (33)$$

We thus conclude (from Eqs. 31 and 33) that

$$\lim_{\epsilon \rightarrow 0} \left(\frac{Sal(\rho + \epsilon\phi)^2 - Sal(\rho - \epsilon\phi)^2}{4\epsilon} \right) = \frac{r'(0)}{4} = f_\rho^T \phi. \quad (34)$$